JAAS

PAPER

A UV digital micromirror spectrometer for dispersive AFS: spectral interference in simultaneous determination of Se and Pb

Chen Tao, [a] Chunsheng Li, *[a] Yingchao Li, [a] Hongxia Wang, [a] Yaru Zhang, [a] Zhiheng Zhou,[b] Xuefei Mao, [c] Zhenyu Ma [d] and Di Tian *[a]

Hollow cathode lamps (HCLs) are excitation light sources commonly used in hydride generation atomic fluorescence spectrometry (HG-AFS). There are obvious Pb interfering lines at 217.0 nm, 261.3 nm, and 283.3 nm in the atomic fluorescence spectrum excited by Se HCLs. This will induce erroneously measured results especially when using the non-dispersive detection method when Se and Pb are detected simultaneously. To solve the spectral interference caused by Se HCLs, in this paper, a UV digital micromirror spectrometer using a digital micromirror device (DMD) as a spatial light modulator, a grating as a spectroscope, and a photomultiplier tube (PMT) as a detector is designed for dispersive atomic fluorescence spectrometry. In addition, a modified DMD with a cover window made of Corning HPFS® 7980 standard grade fused silica was used to provides a higher transmittance of 180–320 nm. The most attractive features of this UV digital micromirror spectrometer are its simple structure, high sensitivity, no macroscopic moving parts, and rapid spectral analysis (0.419 s per spectrum). After optimizing DMD and PMT control parameters, the effects of the chemical generation system ($K_3Fe(CN)_6$, KBH_4, and HCl) are investigated. The atomic fluorescence spectra of Se and Pb are obtained, and the detection limits of the analytical lines are discussed. The feasibility of the present method is confirmed by simultaneous detection of Se and Pb using water samples (GSBZ50031-94 and GSB07-1183-2000) and multi-element standard solution (GBW(E)080669) as reference materials. This study demonstrates the potential of the proposed spectrometer for dispersive HG-AFS, which appropriately reduces the purity requirements of the light source and the spectral interference from light sources. It is also applicable to simultaneous detection using multi-element HCLs or continuous light sources.

Introduction

Se is an essential element for human health at low concentrations while exhibiting detrimental effects when exceeding a certain threshold.[1–3] Meanwhile, Pb is regarded as one of the most threatening environmental contaminants because of its long persistence in soil and high toxicity to plants, animals, and humans.[4,5] While more and more selenium-enriched foods, agricultural products, and drinking water[6] are considered to be beneficial to the human body and are widely used, simultaneous detection of Pb has also received extensive attention. The methods available for simultaneous determination of Se and Pb include atomic absorption spectroscopy (AAS),[7] hydride generation atomic fluorescence spectrometry (HG-AFS),[8–11] inductively coupled plasma–mass spectrometry (ICP-MS),[12–14] *etc.* Atomic fluorescence spectrometry (AFS) has proven extremely useful owing to its high sensitivity,[15–17] low cost, and precise determination at trace levels.[18–21] Hollow cathode lamps (HCLs) are the most widely used intense, narrow line sources employed in atomic fluorescence instrumentation.[22] Experiments found that there are obvious Pb interfering lines at 217.0 nm, 261.3 nm, and 283.3 nm in the atomic fluorescence spectrum excited by Se HCLs; these lines may introduce detection errors. This occurs especially when using the non-dispersive detection method, where Se and Pb are detected simultaneously.

Since most AFS analytical lines are within the range of 180–320 nm, CCD spectrometers are not useful for the trace detection owing to their low sensitivity in this (deep UV) range. Recently, a new approach that uses a digital micromirror device (DMD), a micro-opto-electro-mechanical system semiconductor device, to control the paths of dispersed spectral lines toward a single detector[23] has gained attention. The DMD is an ideal device to use as a spatial light modulator (SLM)[24,25] for

[a] *College of Instrumentation & Electrical Engineering, Jilin University, Changchun 130023, China. E-mail: tiandi@jlu.edu.cn*

[b] *Beijing Bohui Innovation Optoelectronic Technology Co., Ltd, Beijing 102206, China*

[c] *Grating Technology Laboratory, Changchun Institute of Optics and Fine Mechanics and Physics, Chinese Academy of Sciences, Changchun 130033, China*

[d] *Institute of Quality Standard and Testing Technology for Agro-Products, Chinese Academy of Agricultural Sciences, Beijing 100081, China*

wavelength selection. Each mirror can rotate in opposite directions at very high speeds. The first use of a DMD in a visible spectrometer was documented and published by Wagner *et al.*[26] in 1995. Since then, it has been effectively used in Raman spectrometers[27,28] and Hadamard transform near-infrared spectrometers.[29–31] The DMD has also been successfully incorporated into flame atomic absorption and emission spectrometry.[32–34]

Although the DMD has proven to be a promising SLM for spectral analysis in the long-wavelength UV range, the most common type of borosilicate glass used in the UV DMD used here (Corning 7056 glass) has 0% optical transmission below 250 nm.[35] In the experiment described in this paper, a UV digital micromirror spectrometer based on the use of a DMD as a light modulator, a concave flat field grating as a spectroscope, and a PMT as a detector was specifically designed for dispersive AFS. Furthermore, a modified DMD with the cover window replaced by glass made of Corning HPFS® 7980 standard-grade fused silica[36] was used, which can provide high transmittance in the range of 180–320 nm. In this paper, the atomic fluorescence spectra of Se and Pb were obtained, and the detection limits of the main analytical lines were discussed. We present a new approach to realize the simultaneous detection of Se and Pb without the spectral interference caused by HCLs.

Experimental

UV digital micromirror spectrometer

A picture of the UV digital micromirror spectrometer is shown in Fig. 1. First, the atomic fluorescence signal passes through a slit (800 μm in height and 100 μm in width), after which it is dispersed by a concave flat field grating (1000 grooves per mm grating, $f = 30$ mm, Changchun Institute of Optics, Fine Mechanics and Physics, China) and projected onto the modified DMD (0.7 XGA DMD, Texas Instruments, USA; the cover window
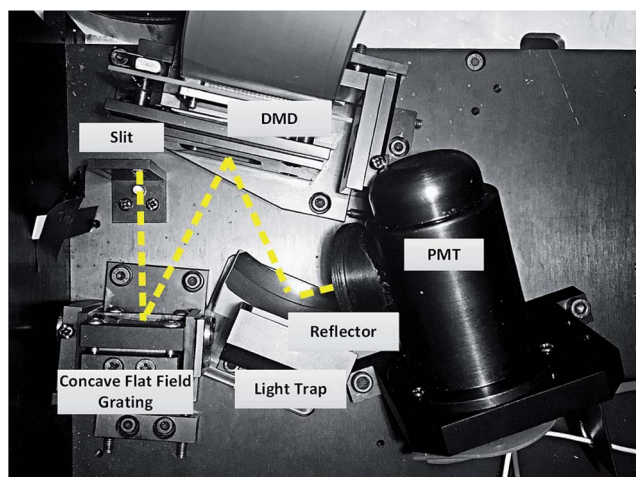

Fig. 1 Photograph of the UV digital micromirror spectrometer. DMD: digital micromirror device; PMT: photomultiplier tube. Additionally, a light shield is used to prevent environmental light from interfering with the spectrometer.
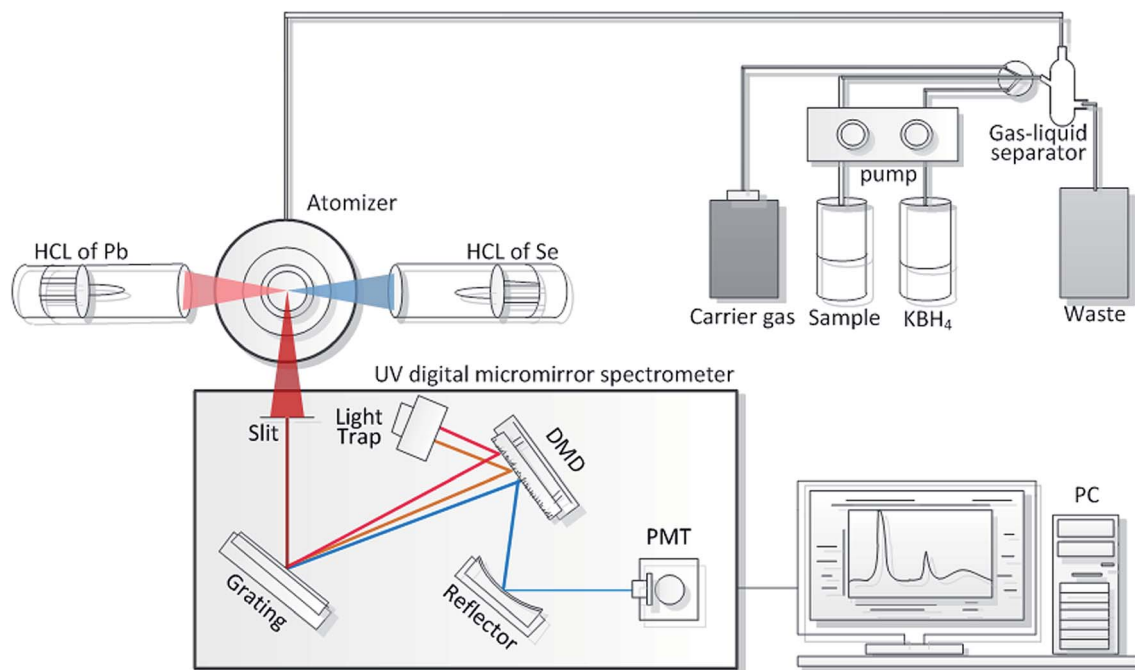
was replaced by Corning HPFS® 7980 standard-grade fused silica modified by the Changchun Institute of Optics, Fine Mechanics and Physics, China). The DMD is used to position the micromirrors in a straight line prior to using a grating to modulate the fluorescence spectral radiation. Each micromirror is controlled by a W4100 development kit (Wintech Technology Development Co., Ltd., Beijing, China) that can rotate it +12° (ON state) or −12° (OFF state) from the neutral position. When the micromirrors are in the ON position, the corresponding fluorescence signal within the wavelength range is sent to the PMT (R7154, Spectral response range 160–320 nm, Hamamatsu, Japan). While in the OFF position, the signal is sent to a light trap (Changchun Institute of Optics, Fine Mechanics and Physics, China) with a light-absorbing material (TB4, Thorlabs, USA) inside.

Experimental setup

A platform consisting of a modified SA-7800 AFS (Beijing Bohui Innovation Optoelectronic Technology Co., Ltd., China) was employed in this experiment, where the non-dispersive detector (PMT) was replaced by the UV digital micromirror spectrometer. A schematic diagram of the experimental setup is shown in Fig. 2. A Pb HCL and 10 Se HCLs (General Research Institute for Nonferrous Metals, Beijing, China) were used as the radiation sources. Another complete SA-7800 AFS was used for non-dispersion comparison experiments.

The sample was first mixed with hydrochloric acid followed by potassium borohydride (KBH_4) to form hydrides. The gaseous hydride formed by the reaction was separated by using a gas–liquid separator, transferred by argon gas, and atomized using a hydrogen diffusion flame generated by excess H_2 generated by the reaction of KBH_4 and hydrochloric acid. The main analytical conditions for the dispersive and non-dispersive experimental setup, including the flow rates of gas and reagent, concentration of samples, *etc.*, are listed in Table 1.

Software

The main control parameters of the system, including DMD control, time taken for signal acquisition, negative high voltage of the PMT, flow rates of samples, lamp primary/boost current of HCLs, *etc.*, were set using in-house routines written in MATLAB 2014a. The routines of data collection and pre-processing were also written within this program, which finally enabled the spectrograms to be plotted on the screen.

Reagents and solutions

All the reagents and water used in the present work were of analytical grade. The standard solutions of Se and Pb were prepared just before use by dilution of the stock solutions (National Research Center for Certified Reference Material, China), and were stored at 4 °C in the dark. Water samples (GSBZ50031-94 and GSB07-1183-2000) and a multi-element standard solution (GBW(E)080669) were prepared for sample analysis. A mixed solution of Se and Pb was prepared by appropriate dilution of the standard sample solution in the range of 2–200 μg L^{-1} (for linear range investigation). Working

This journal is © The Royal Society of Chemistry 2018

J. Anal. At. Spectrom., 2018, **33**, 2098–2106 | **2099**

Fig. 2 Schematic diagram of the experimental setup.

Table 1 Main analytical conditions in the experimental setup

Parameters	Setting value (by the UV digital micromirror spectrometer method)	Setting value (by the non-dispersive method)
Flow rate of carrier gas	400 mL min⁻¹	400 mL min⁻¹
Flow rate of shield gas	850 mL min⁻¹	850 mL min⁻¹
KBH₄ concentration	1.6 g L⁻¹	1.6 g L⁻¹
HCl concentration	3 mol L⁻¹	3 mol L⁻¹
K₃Fe(CN)₆ concentration	2.5 g L⁻¹	2.5 g L⁻¹
Sample flow rate	0.1 mL s⁻¹	0.1 mL s⁻¹
Reductant flow rate	0.05 mL s⁻¹	0.05 mL s⁻¹
Lamp primary/boost current of Se	60 mA/30 mA	60 mA/30 mA
Lamp primary/boost current of Pb	60 mA/30 mA	60 mA/30 mA
Negative high voltage of PMT	450 V	280 V

standard solutions of Se, Pb, and their mixtures were prepared daily by stepwise dilution of the stock solutions just before use. The $K_3Fe(CN)_6$ (Sinopharm Group Chemical Reagent Co., Ltd.) and KBH_4 (Tianjin Institute of Chemical Reagents, Tianjin, China) solution were prepared by dissolving KBH_4 in a 0.5% (m/v) NaOH solution (Beijing Chemicals Co., China). Argon (99.99%) (Praxair Inc., Beijing, China) was used as the carrier gas and the shield gas.

Results and discussion

Control parameters of the UV digital micromirror spectrometer

Rotation parameters of the DMD. The lines of digital micromirrors can be set and rotated together to create a structure similar to an "exit slit". There are four main control parameters including the scanning range, simultaneous rotating lines, interval lines, and wait time which need to be studied and optimized. The schematic diagram of the control mode of the DMD is shown in Fig. 3. The atomic fluorescence intensity and the shape of the peaks can be altered by the variation of the "exit slit".

Scanning range. Because the grating is designed to divide the wavelengths nearly equally and project them onto the DMD, the relationship between the lines of the DMD and wavelength satisfies the approximate formula $\lambda^2 = -3 \times 10^{-5}C^2 + 0.195C + 174.25$, where λ is the wavelength and C is the number of lines of the DMD. Every single line of the digital micromirrors corresponds to different regions of the wavelength, and the wavelength error is less than 0.5 nm. The scanning range was
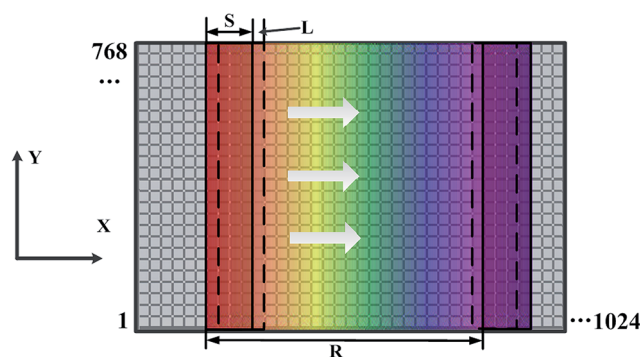

Fig. 3 Control mode of the DMD; the rotating action starts from left to right: 'S' means simultaneous rotating line; 'L' means interval line; 'R' means scanning range. The colored zone represents the dispersed spectrum, which was projected from the grating.

2100 | J. Anal. At. Spectrom., 2018, **33**, 2098–2106

This journal is © The Royal Society of Chemistry 2018

set to start from line 2 to the end of line 840, which can achieve a detection region from approximately 180 to 320 nm.

Simultaneous rotating and interval lines. The increase in the number of simultaneous rotating lines could lead to higher fluorescence intensity and wider peaks. The influence of simultaneous rotating lines of the Pb peak at 261.3 nm is shown in Fig. 4 as an example. With the increase in the scanning bandwidth, the relative position of the peaks would be shifted. The peak shifting of the spectrum would occur (approximately 0–7.63 line numbers of the DMD shift from 1 to 16 lines). The rotating lines move several lines backward after every rotating action. The maximum sampling density can be obtained when one line is set (Fig. 5a). With the increase in the number of interval lines (Fig. 5b–d), the peak shape and intensity relationships become increasingly inaccurate and unreliable.
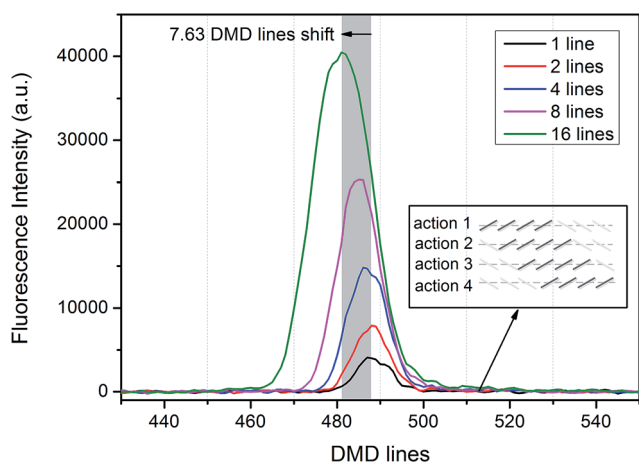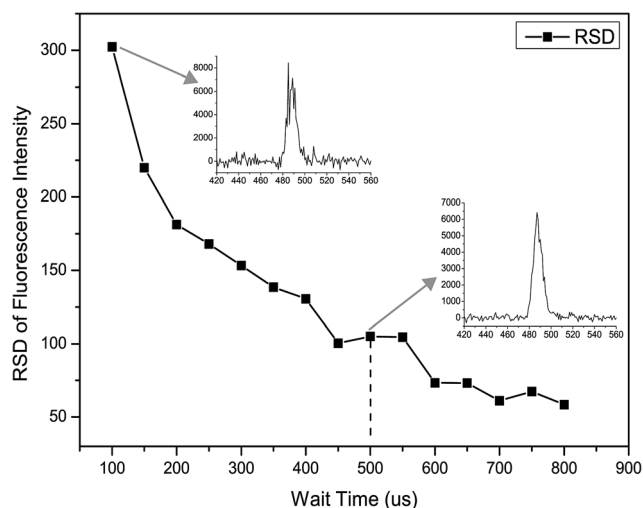

Fig. 6 Effect of the relationship between the wait time and RSD of fluorescence intensity.

Wait time. Some interval is necessary between the rotational actions of the DMD in order for it to be compatible with light source modulation and signal acquisition. The sampling frequency is 1 MHz, and the fluorescence signal is constantly being superimposed during the wait time, as shown in Fig. 6. With the increase in the wait time, the relative standard deviation (RSD) of fluorescence intensity is reduced. Meanwhile, the consumption of the sample increases gradually; selecting 500 μs is a compromise. The actual scanning time was 0.419 s (838 lines × 500 μs) for every single detection process from 180 to 320 nm. The rotation parameters of the DMD are listed in Table 2.

Negative high voltage of the PMT. The relationship between signal intensity and the negative high voltage of the PMT is shown in Fig. 7. The results demonstrated that the fluorescence
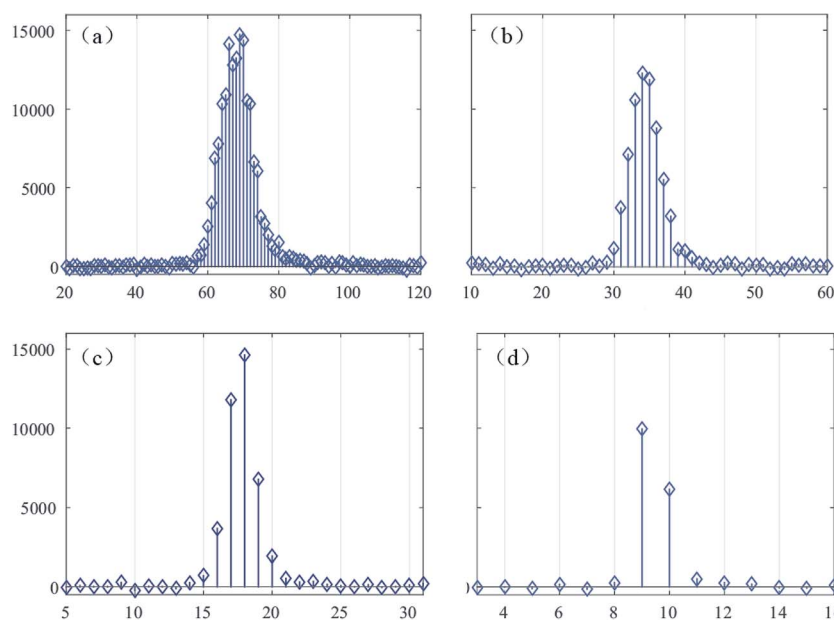

Fig. 4 Effect of the rotating line number of the DMD (1–16 lines) on the intensity of the fluorescence signal of Pb at 261.3 nm.

Fig. 5 Effect of interval lines of the DMD: (a) one interval line; (b) two interval lines; (c) four interval lines; (d) eight interval lines.

This journal is © The Royal Society of Chemistry 2018

J. Anal. At. Spectrom., 2018, 33, 2098–2106 | 2101

Table 2   Rotation parameters of the DMD

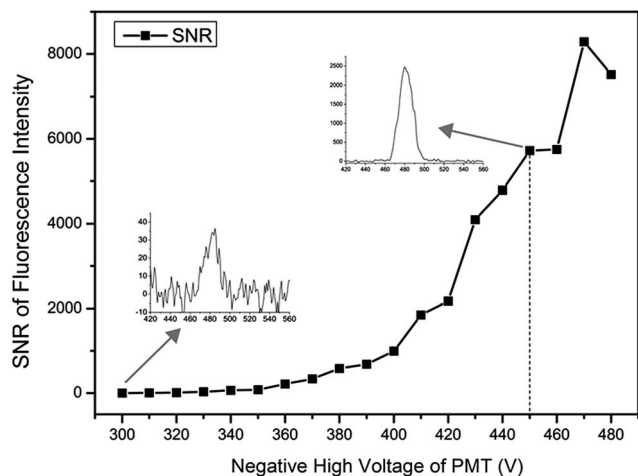| Scanning line range	Wavelength range (nm)	Simultaneous rotating lines	Interval lines	Wait time
2–840	180–320	16 lines	1 line	500 μs

Fig. 7   Relationship between the SNR and the negative high voltage of the PMT.

signal gradually increased as the negative high voltage increased from 300 to 480 V. The signal was unstable and the noise drifted evidently when the negative high voltage was above 450 V.

Analysis of characteristic lines

Excitation spectra of Se and Pb HCLs. Since the intensity of the Se and Pb emission lines is too strong, the condition parameters had to be adjusted, including the lamp primary/boost current (both Se and Pb HCLs, 30 mA/15 mA) and the negative high voltage of the PMT (400 V) when we detected the spectra of Se and Pb HCLs. As shown in Fig. 8, it was found that some emission lines of the Se HCL overlap with those of Pb: for
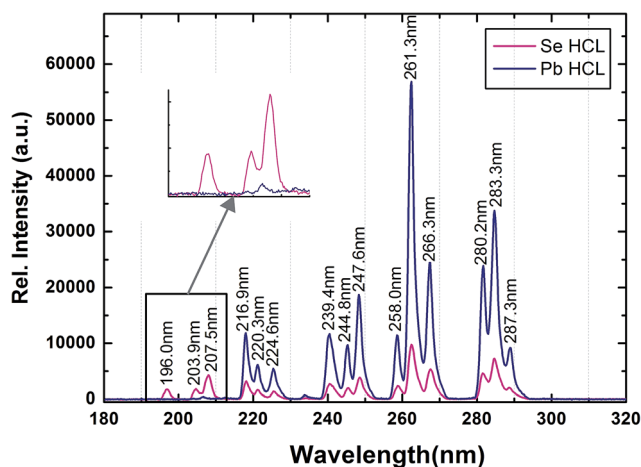

Fig. 8   Spectra of HCLs between Se and Pb.

example, at 216.9 nm, 247.6 nm, and 264.1 nm, *etc.* The main reason for this problem may be that the melting point of SePb (1065 °C), as the cathode, is much higher than that of Se (217 °C). SePb can withstand greater current excitation and provide longer service life, but Se and Pb are excited simultaneously.

Fluorescence spectra of Se and Pb HCLs. To minimize background noise from the argon emission of the flame and to avoid reflected radiation from the light source found elsewhere, fluorescence was detected at the outlet of the atomizer and collected by the spectrometer at an angle of 90° to the Se and Pb HCLs. Fig. 9 shows the spectra of Se and Pb with the mixed standard solution (100 μg mL^{-1} Se and 100 μg mL^{-1} Pb). Pb has three characteristic lines at 217.0 nm, 261.3 nm, and 283.3 nm. Se should have characteristic lines only at 196.0 nm and 203.9 nm. However, characteristic lines were also observed at the fluorescence lines of Pb, where the fluorescence intensity was much less than the characteristic lines excited by the Pb HCL. The experimental results further verify the existence of spectral interference; the main reason for this phenomenon is that the Se HCL contains a certain amount of Pb.

Spectral interference comparison of ten Se HCLs. The results of comparative experiments on ten different Se HCLs at three positions (217.0 nm, 261.3 nm, and 283.3 nm) can be seen in Fig. 10. Each lamp contains a certain amount of Pb; moreover, there are some degrees of difference among the fluorescence intensities. This may be because the Pb content was different in every Se HCL. One of these Se HCLs was chosen for the next experiment.

Chemical generation system

KBH$_4$ concentration. The KBH$_4$ concentration is a major factor that has a definitive effect on hydride generation performance. If the concentration of KBH$_4$ is too low, the hydride reaction of the measured element may be incomplete and a poor fluorescence intensity value may be obtained. If the concentration of KBH$_4$ is too great, excessive hydrogen may be generated and the Se hydride gas may be diluted, reducing the
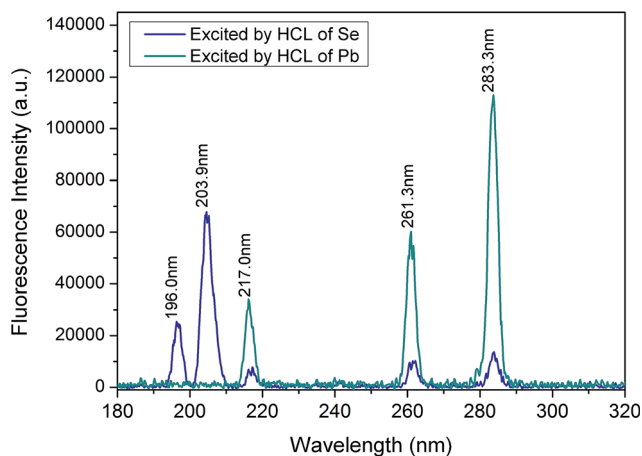

Fig. 9   Spectra of Se and Pb; characteristic lines of Se at 196.0 nm and 203.9 nm (blue line); characteristic lines of Pb at 217.0 nm, 261.3 nm, and 283.3 nm (green line).
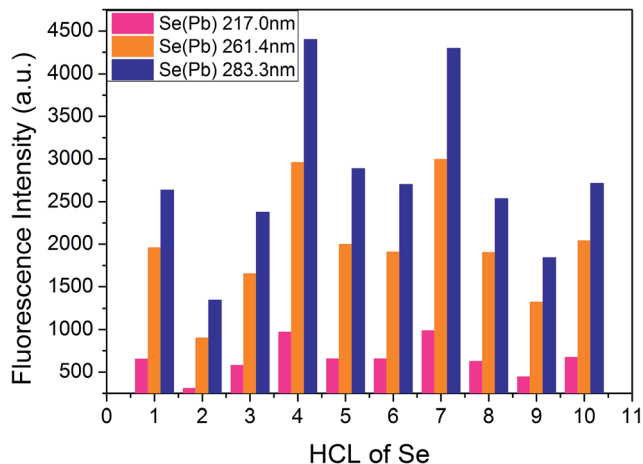
Fig. 10 Relationship between fluorescence intensity at 217.0 nm, 261.3 nm, and 283.3 nm obtained from 10 different Se HCLs; fluorescence intensity at 217.0 nm (pink bar); fluorescence intensity at 261.4 nm (orange bar); fluorescence intensity at 283.3 nm (blue bar).

fluorescence intensity; the latter is probably due to continuously increasing dilution of the analyte by the generated hydrogen and the reduced residence time of the analyte species in the atomizer.[37] In this experiment, the KBH_4 concentration was investigated from 0.8 to 2.0% (w/v) in a 0.5% NaOH medium. Fig. 11 shows the fluorescence intensity of Se and Pb variation *versus* potassium borohydride concentration. The results indicate that Se performance observed at a KBH_4 concentration of 1.6% (w/v) is preferably an excitation effect; at the same time, Pb is manifested first and the trend continues to grow. Therefore, a KBH_4 concentration of 1.6% (w/v) is the optimum condition for simultaneous detection of Se and Pb.

HCl concentration. HCl concentration is another key parameter for hydride generation; hence, the effect of the concentration of HCl on the detection of the elements was investigated under optimized conditions of the simultaneous detection of Se and Pb. As can be seen in Fig. 12, the signal increased with increasing HCl concentration from 2% to 7% for Se. Higher concentration was unfavourable for Pb excitation. Using 3% (w/v) HCl is suitable for simultaneous determination of Se and Pb, and the reaction system is stable.

$K_3Fe(CN)_6$ concentration. $K_3Fe(CN)_6$ is added as an oxidant to oxidize Pb(II) to Pb(IV). The unstable neo-ecological Pb(IV) rapidly forms a stable compound with $Fe(CN)_6^{3-}$, and the complex is also reduced by KBH_4 to form a hydride. In this experiment, the $K_3Fe(CN)_6$ concentration was investigated from 0 to 1.0% (w/v). Fig. 13 shows that increasing the concentration of $K_3Fe(CN)_6$ favours the signal of Pb. The observation of Se

Fig. 11 Effect of optimization of the KBH_4 concentration on the fluorescence signal (Se at 196.0 nm and 203.9 nm: green lines; Pb at 217.0 nm, 261.3 nm, and 283.3 nm: blue lines).
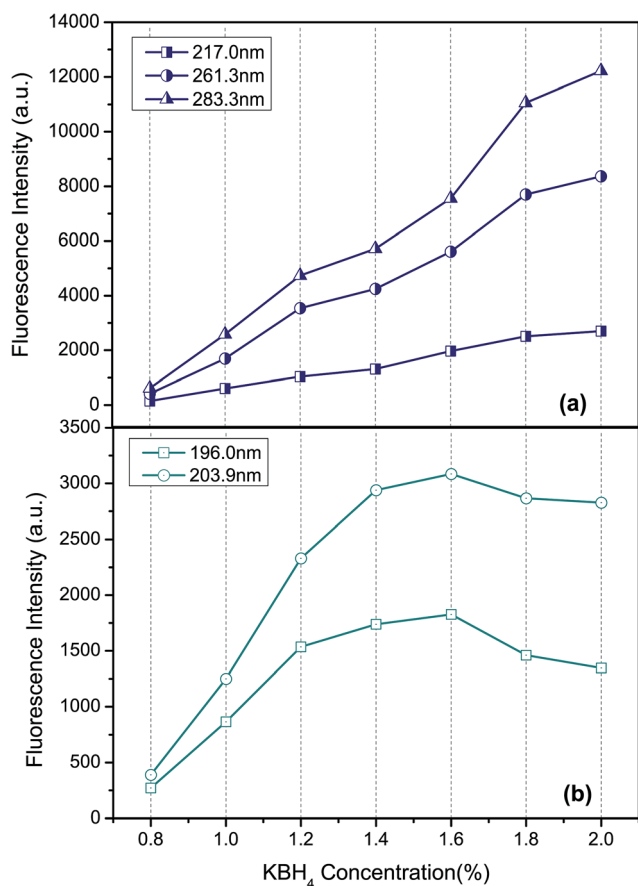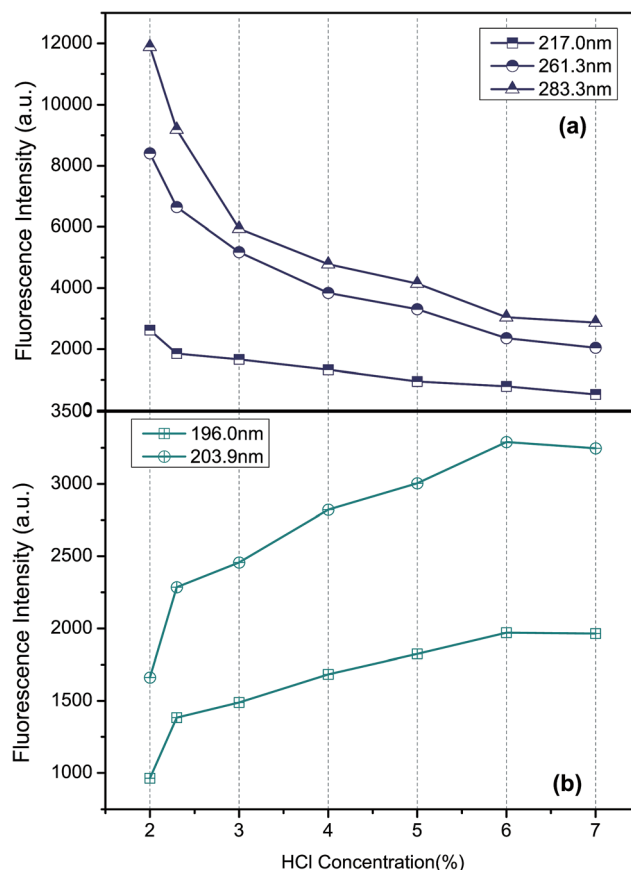

Fig. 12 Effect of optimization of the HCl concentration on the fluorescence signal (Se at 196.0 nm and 203.9 nm: green lines; Pb at 217.0 nm, 261.3 nm, and 283.3 nm: blue lines).
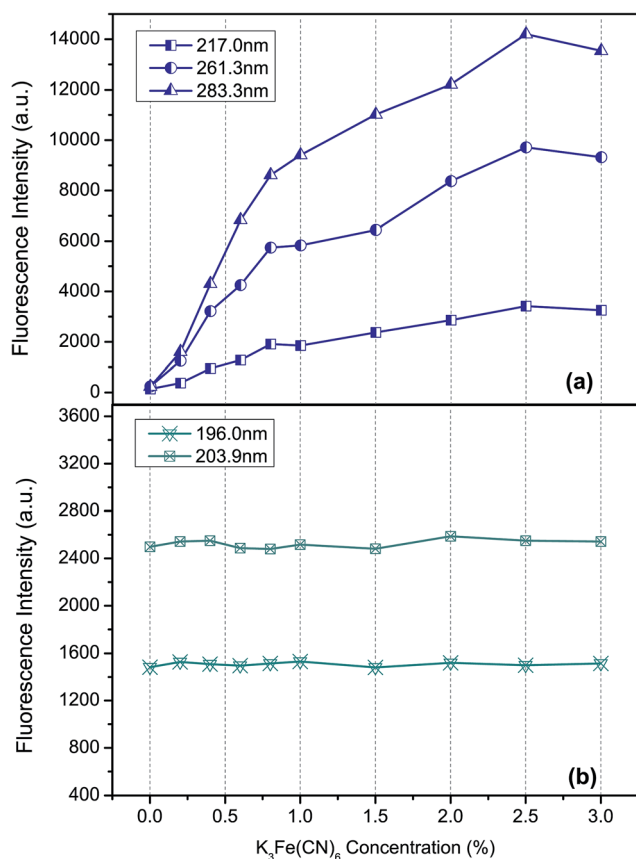
This journal is © The Royal Society of Chemistry 2018

J. Anal. At. Spectrom., 2018, **33**, 2098–2106 | **2103**

Fig. 13 Effect of optimization of the $K_3Fe(CN)_6$ concentration on the fluorescence signal (Se at 196.0 nm and 203.9 nm: green lines; Pb at 217.0 nm, 261.3 nm, and 283.3 nm: blue lines).

signals at 196.0 nm and 203.9 nm indicates that Se is not affected by changes in $K_3Fe(CN)_6$ concentration. Taken together, the experimentally selected actual $K_3Fe(CN)_6$ concentration is 2.5% (w/v).

Analytical performance

The limits of detection (LOD $= 3S_{blank}/b$) and quantification (LOQ $= 10S_{blank}/b$) were estimated according to IUPAC recommendations.[38,39] S_{blank} is the standard deviation of the blank measurement and b is the angular coefficient of the analytical curve. The LODs and LOQs of the main analytical lines of Se and Pb were obtained for concentrations ranging from 2 to 200 µg L^{-1} via the peak area measurement method. The peaks

of all samples were plotted from an average of 50 accumulated spectra.

The analytical performance of the UV digital micromirror spectrometer was investigated with respect to the characteristic lines at 203.9 nm (Se) and 283.3 nm (Pb). The curve parameters of the linear model constructed ($y = \alpha + \beta x$) were $\alpha = 843.06$ and $\beta = 3355.71$ for Se, and $\alpha = 774.01$ and $\beta = 7076.65$ for Pb. The limit of detection (LOD) and the limit of quantification (LOQ) of Se at 203.9 nm were estimated at 0.89 µg L^{-1} and 2.97 µg L^{-1} concentrations with a correlation coefficient of $r = 0.9975$, and those for Pb at 283.3 nm were estimated at 0.42 µg L^{-1} and 1.4 µg L^{-1} concentrations with a correlation coefficient of $r = 0.9987$. The dispersive detection method of the UV digital micromirror spectrometer gave an LOD of Se close to that obtained using ion pairing liquid chromatography-microwave assisted HG-AFS,[40] and Pb using graphite furnace atomic absorption spectrometry.[41] The detection limits of the main analytical lines of Se and Pb and the spectral characteristics of important analytical lines, including the relationship of the relative fluorescence intensity and the relative emission intensity of the light source, were calculated and tabulated (Table 3) from the calibration data.

The repeatability of the dispersive detection method using the UV digital micromirror spectrometer was also evaluated using a 20 µg L^{-1} standard solution mixture of Se and Pb under the same conditions, *i.e.* the same method, same material, same operator, same laboratory, and short time between measurements. The results showed that the relative standard deviations were 2.18% (20 µg L^{-1}, Se, $n = 9$) and 1.66% (20 µg L^{-1}, Pb, $n = 9$). At the same time, the repeatability was verified by a one-sample t-test. The results were evaluated as $p = 0.55$ for Se and $p = 0.723$ for Pb; the results from the t-test at a 95% confidence level with eight degrees of freedom revealed that the results presented no significant differences.

Validation and sample analysis

To demonstrate the analytical accuracy of the present method. The non-dispersive methods and the present method were applied for the determination of Se and Pb in water samples (GSBZ50031-94 and GSB07-1183-2000) and multi-element standard solution (GBW(E)080669) as reference materials. The analytical results are given in Table 4. Recovery tests were performed with 40 µg mL^{-1} Se and 40 µg mL^{-1} Pb added to these three samples, and the results are shown in Table 5. The sample measurements ($n = 3$) were always accomplished on the same

Table 3 Analytical results for Se and Pb in standard samples

Element	Wavelength (nm)	Relative fluorescence intensity (%)	Linear range (µg L^{-1})	Relative coefficient	Detection limit (µg L^{-1})
Se	196.0	100	4–200	0.9984	2.05
	203.9	42.83	2–200	0.9963	0.89
Pb	217.0	29.35	4–200	0.9978	1.46
	261.3	52.84	2–200	0.9987	0.94
	283.3	100	2–200	0.9991	0.42

Table 4 Analytical results (means $\pm$ s, $n = 3$) for Se and Pb in samples

Standard Sample	Certified value ($\mu g\ L^{-1}$)		Found by the non-dispersive method ($\mu g\ L^{-1}$)		Found by the UV digital micromirror spectrometer method ($\mu g\ L^{-1}$)	
	Se	Pb	Se	Pb	Se	Pb
GSBZ50031-94	47.5	0	33.85 ± 0.41	0.13 ± 0.18	46.92 ± 0.89	0.47 ± 0.43
GSB07-1183-2000	0	62.38	17.56 ± 0.36	63.64 ± 0.44	-0.28 ± 0.27	63.47 ± 1.53
GBW(E)080669	100	100	101.34 ± 0.43	99.54 ± 0.65	99.32 ± 2.21	101.35 ± 2.84

Table 5 Recovery results (means $\pm$ s, $n = 3$) of Se and Pb in samples

Standard sample	Spiked ($\mu g\ L^{-1}$)		Recovery by the non-dispersive method (%)		Recovery by the UV digital micromirror spectrometer method (%)	
	Se	Pb	Se	Pb	Se	Pb
G1	47.5 + 40	0 + 40	71.32 ± 1.54	102.1 ± 1.65	98.74 ± 1.74	101.15 ± 2.18
G2	0 + 40	62.38 + 40	57.07 ± 2.11	99.33 ± 1.94	101.93 ± 1.92	98.64 ± 2.31
G3	100 + 40	100 + 40	101.51 ± 1.37	93.07 ± 1.78	102.08 ± 1.84	99.86 ± 2.33

Table 6 P value by obtained the paired t-test ($n = 3$) for the two detection methods

P value	GSBZ50031-94	GSB07-1183-2000	GBW(E)080669	G1	G2	G3
$P(Se)$	0.003 < 0.005	0.000 < 0.005	0.244	0.000 < 0.005	0.000 < 0.005	0.23
$P(Pb)$	0.140	0.908	0.851	0.126	0.507	0.607

day and submitted to the same analytical process in order to avoid calibration errors.

As a result, the determined concentrations of Se and Pb using the UV digital micromirror spectrometer method were in agreement with the certified values. The recovery factor was found to be between 97% and 104% for Se and 96% and 103% for Pb. The detection results for Se, using the non-dispersive method, were significantly affected when Pb was contained in the samples. This fact may be explained based on the influence of spectral interference of Pb in the Se HCL. In addition, statistical tests were accomplished in order to verify the accuracy of the method. A paired t-test was performed for the two methods at a confidence level of 95%, and the P value obtained is listed in Table 6. The results also showed significant differences for the detection of Se, but both methods provided similar results for Pb, showing no statistically significant differences.

Conclusions

The UV digital micromirror spectrometer described in this paper provides a new method of dispersive detection for atomic fluorescence spectrometry. The most attractive characteristics of the present spectrometer are its simple structure, high sensitivity, no macroscopic moving parts, and rapid spectral analysis (0.419 s per sample). They allow it to avoid spectral interference caused by HCLs and facilitate extension of the application types and range of light sources. It has been applied for simultaneous detection of Se and Pb in this study and the results verified that the proposed spectrometer can avoid the spectral interference of Se HCLs.

In summary, based on the primary results of this study, we can conclude that the UV digital micromirror spectrometer has the potential to become the preferred instrument in some types of UV spectral analysis applications. It may also lend itself well to the development of portable instruments and possible advances in detection techniques. To achieve better sensitivities for simultaneous detection of Se and Pb, a further increase in performance can be expected by improving the design of the detection and acquisition system. This could involve, for example, using a better PMT or electrodeless discharge lamps to provide higher sensitivity and lower detection limits (by about 1–2 orders of magnitude). The optimization of the control method for the DMD is also a good way, including accurate detection of the characteristic lines by designing a special scanning control technology: for example, replacing existing line control with pixel control of the DMD. The proposed approach can further realize fast multi-element simultaneous detection using multi-element HCLs or continuum source excitation.

Conflicts of interest

The authors report that there are no conflicts of interest.

Acknowledgements

References

1 G. N. Schrauzer and D. A. White, *Bioinorg. Chem.*, 1978, **8**, 303–318.

2 H. F. Mayland, W. T. Frankenberger Jr and S. Benson, *Selenium in the Environment*, 1994, pp. 29–45.

3 K. M. Peters, S. E. Galinn and P. A. Tsuji, *Selenium: Dietary Sources, Human Nutritional Requirements and Intake across Populations*, Springer International Publishing, 2016.

4 S. H. M. PhD, *Am. J. Ind. Med.*, 2000, **38**, 244–254.

5 N. Zheng, Q. Wang and D. Zheng, *Sci. Total Environ.*, 2007, **383**, 81–89.

6 C. Y. Lu, X. P. Yan, Z. P. Zhang, Z. P. Wang and L. W. Liu, *J. Anal. At. Spectrom.*, 2004, **19**, 277–281.

7 R. M. D. Oliveira, A. C. N. Antunes, M. A. Vieira, A. L. Medina and A. S. Ribeiro, *Microchem. J.*, 2016, **124**, 402–409.

8 Z. Long, Y. Luo, C. Zheng, P. Deng and X. Hou, *Appl. Spectrosc. Rev.*, 2012, **47**, 382–413.

9 Z. Long, C. Chen, X. Hou and C. Zheng, *Appl. Spectrosc. Rev.*, 2012, **47**, 495–517.

10 Z. Zhu, J. Liu, S. Zhang, X. Na and X. Zhang, *Spectrochim. Acta, Part B*, 2008, **63**, 431–436.

11 F. Wang and G. Zhang, *Appl. Spectrosc.*, 2011, **65**, 315–319.

12 M. A. Vieira, A. S. Ribeiro and A. J. Curtius, *Microchem. J.*, 2006, **82**, 127–136.

13 C. Tănăselia, T. Frențiu, M. Ursu, M. Vlad, M. Chintoanu, E. A. Cordos, L. David, M. Paul and D. Gomoiescu, *Optoelectron. Adv. Mater., Rapid Commun.*, 2008, **2**, 99–107.

14 C. Li, Z. Long, X. Jiang, P. Wu and X. Hou, *Trends Anal. Chem.*, 2016, **77**, 139–155.

15 J. Jia, Z. Long, C. Zheng, X. Wu and X. Hou, *J. Anal. At. Spectrom.*, 2015, **30**, 339–342.

16 H. Ke, K. Xu, Z. Wei, Y. Lu, X. Hou and C. Zheng, *Anal. Chem.*, 2015, **88**, 789.

17 D. R. Jones, J. M. Jarrett, D. S. Tevis, M. Franklin, N. J. Mullinix, K. L. Wallon, D. Q. C. Jr, K. L. Caldwell and R. L. Jones, *Talanta*, 2017, **162**, 114–122.

18 Z. Zou, Y. Deng, J. Hu, X. Jiang and X. Hou, *Anal. Chim. Acta*, 2018, **1019**, 25–37.

19 D. J. Butcher, *Appl. Spectrosc. Rev.*, 2016, **51**, 397–416.

20 D. Sánchezrodas, W. T. Corns, B. Chen and P. B. Stockwell, *J. Anal. At. Spectrom.*, 2010, **25**, 933–946.

21 Y. K. Lu, H. W. Sun, C. G. Yuan and X. P. Yan, *Anal. Chem.*, 2002, **74**, 1525–1529.

22 H. Morgner, M. Neumann, S. Straach and M. Krug, *Surf. Coat. Technol.*, 1998, **108–109**, 513–519.

23 H. Liu and B. Bhushan, *Ultramicroscopy*, 2004, **100**, 391.

24 J. N. Chen, *US Pat.*, 20050157370 A1, 2005.

25 S. M. Penn, *US Pat.*, 7961399, 2011.

26 E. P. Wagner, B. W. Smith, S. Madden, J. D. Winefordner and M. Mignardi, *Appl. Spectrosc.*, 1995, **49**, 1715–1719.

27 N. T. Quyen, E. Da Silva, N. Q. Dao and M. D. Jouan, *Appl. Spectrosc.*, 2008, **62**, 273–278.

28 Z. J. Smith, S. Strombom and S. Wachsmann-Hogiu, *Opt. Express*, 2011, **19**, 16950–16962.

29 B. Hu, D. Feng and J. Xu, *Appl. Spectrosc.*, 2012, **66**, 1044–1052.

30 J. L. Xu, H. Liu, C. B. Lin and Q. Sun, *Opt. Commun.*, 2017, **383**, 250–254.

31 D. Xiang and M. A. Arnold, *Appl. Spectrosc.*, 2011, **65**, 1170–1180.

32 J. D. Batchelor and B. T. Jones, *Anal. Chem.*, 1998, **70**, 4907–4914.

33 J. D. Usala, A. Maag, T. Nelis and G. Gamez, *J. Anal. At. Spectrom.*, 2016, **31**, 2198–2206.

34 T. M. Spudich, C. K. Utz, J. M. Kuntz, R. A. Deverse, R. M. Hammaker and D. L. Mccurdy, *Appl. Spectrosc.*, 2003, **57**, 733.

35 R. E. Williams and B. M. Callies, *US Pat.*, 7161727 B2, 2007.

36 M. A. Quijada, A. Travinsky, D. Vorobiev, Z. Ninkov, A. Raisanen, M. Robberto and S. Heap, Advances in Optical and Mechanical Technologies for Telescopes and Instrumentation II, *Spie-Int Soc Optical Engineering*, Bellingham, 2016.

37 I. Novotny, J. C. Farinas, J. L. Wan, E. Poussel and J. M. Mermet, *Spectrochim. Acta, Part B*, 1996, **51**, 1517–1526.

38 A. D. McNaught, A. Wilkinson and International Union of Pure and Applied Chemistry, *Compendium of Chemical Terminology: IUPAC Recommendations*, Blackwell Science, Oxford, England, 2nd edn, 1997.

39 E. M. G. Melo, J. P. A. Fernandes, F. A. S. Cunha, J. O. B. Lira, R. A. C. Lima, K. M. G. Lima and L. F. Almeida, *Anal. Methods*, 2016, **8**, 7047–7053.

40 E. Dumont, K. De Cremer, M. Van Hulle, C. C. Chery, F. Vanhaecke and R. Cornelis, *J. Anal. At. Spectrom.*, 2004, **19**, 167–171.

41 T. M. de Oliveira, P. J. Augusto, F. M. Lurdes and J. K. Cristiane, *Food Chem.*, 2017, **229**, 721.

2106 | *J. Anal. At. Spectrom.*, 2018, **33**, 2098–2106

This journal is © The Royal Society of Chemistry 2018